Audio Engineering Society

Convention Paper

Presented at the 117th Convention
2004 October 28–31 San Francisco, CA, USA

Characterization of Spherical Loudspeaker Arrays

Peter Kassakian[1], and David Wessel[1]*

[1] *Center for New Music and Audio Technologies (CNMAT), UC, Berkeley*

Correspondence should be addressed to Peter Kassakian (kassak@cnmat.berkeley.edu)

ABSTRACT

The synthesis and rotational control of radiation patterns produced by spherical arrays of loudspeakers is studied. We identify operating regions, in terms of complexity of patterns and frequency ranges, over which patterns can be accurately synthesized. By considering an inner product space of far-field patterns, we can reason geometrically about approximation errors when using the systems to synthesize and control target responses. Bounds for normalized error across subspaces, in particular subspaces corresponding to the control operation of rotation, are calculated using singular value decomposition. The bounds can be interpreted as the best and worst case errors encountered when dynamically steering the patterns.

1. INTRODUCTION

In this study we investigate the application of spherical loudspeaker arrays to the synthesis of prescribed spatial radiation patterns. Among other arrays, we consider an existing dodecahedral loudspeaker array, constructed at the Center for New Music and Audio Technologies. The array consists of twelve independently controllable drivers, each with its own isolated enclosure. We are interested in determining the types of radiation patterns that can be generated by the array, and also the types of patterns that can be controlled using the array (for example electronic rotation of a generated pattern).

The ideas presented here are applicable for arrays, designed to simulate complicated point sources, such as icosahedral arrays, cubic arrays, or arrays without any regular symmetry. The systems are constructed for a multitude of uses. See [1] for another study involving such arrays. We refer to these types of arrays as "spherical arrays" or "point-source arrays" to distinguish them from arrays designed either to project in specific directions such as line arrays, or to provide listeners with near–field experiences like surrounding speakers or wavefield synthesis [2].

The desire to control a point–source loudspeaker ar-

*The authors would like to thank Meyer Sound Laboratories, Inc. for continued collaboration and research support.

ray arises in musical instrument synthesis, where the instrumentalist would like to synthesize not only the timbre of the instrument, but the radiation pattern. Point–source loudspeakers are also useful for measurement of the acoustics of rooms and auditoriums, and can provide the engineer easy access to a variety of stimuli, or time–varying stimuli. In many cases a control operation, such as rotation, can be identified with a subspace of radiation patterns. In this report we describe a method for evaluating these types of arrays with respect to their abilities to synthesize prescribed radiation patterns. We are especially interested in characterizing the arrays with respect to their abilities to electronically rotate patterns.

There are a number of practical applications of radiation pattern synthesis and dynamic variation of such patterns. One compelling example involves the electronic simulation of the striking of a gong or tamtam, commonly used percussion instruments, that upon striking produce dipole patterns that rotate most typically in the horizontal plane. Using our dodecahedral array we have produced convincing simulations of the dynamic patterns of struck gongs. More complex examples would include the pattern dynamics caused by the movements of musicians when playing an instrument. Another application of complex and dynamic pattern synthesis occurs in the exploitation of the acoustic properties of rooms. Using adaptive techniques and microphone arrays, most typically a dummy head stereo microphone, we can adjust the patterns dynamically so as to privilege perceptually desirable early reflection patterns from the room. Yet another example involves tracking performers who are using microphones so as to produce nulls or notches in their directions so as to reduce the possibility of feedback. All of these applications will benefit from knowledge of the limits involved in the synthesis of complex patterns and their dynamic manipulation.

By considering target patterns consisting of spherical harmonics at different frequencies, we can generate a corresponding set of errors between the target patterns and the best fitting array–achievable patterns. This set of errors is then the basis for determining what patterns, at what frequencies, can or cannot be reasonably synthesized with the array. By considering an inner–product space of far–field patterns (spanned by the spherical harmonics), we show how one can view this error function from a geometric perspective. For example, the errors are equivalent to angles between vectors. Using this framework, we show that angles between subspaces correspond to best and worst case error bounds for sets of linear combinations of patterns. Linearly combining patterns is an important mechanism for dynamic control.

The emphasis is on the characterization method, which has least–squares optimization at its core. We will describe this in detail, and identify elements that make our application unique. We will then present characterizations of arrays of varying sizes, numbers of drivers, and spatial responses associated with the individual drivers. The conclusions are not surprising: more drivers and smaller spacings in the array produces more control.

2. THEORY

Because loudspeaker arrays consist of a finite number of drivers in a fixed geometry, the (far–field) radiation patterns they can produce are limited to a subset of all the conceivable patterns. For example, a two speaker system could never reproduce the complicated radiation pattern generated by a violin. An arbitrary vibrating body could conceivably possess an arbitrarily complicated radiation pattern at each frequency. We wish to find which types of patterns can be well–approximated using arrays of loudspeakers.

It is convenient to parameterize the set of radiation patterns in terms of spherical harmonics. The spherical harmonics are solutions to the Helmholtz equation, (see Chapter 10 of [3] and also [4]), and span the entire space of physically realizable far–field patterns. Any spatial response then, can be represented by its spherical harmonic expansion as a function of frequency. The decomposition has intuitive appeal, indexing the spatial complexity or "spatial frequency" of radiation patterns.

2.1. Physical System

The loudspeaker array consists of independent loudspeakers arranged in a fixed geometry. The components of the system are i) the pattern produced as a function of frequency, ii) the individual loudspeaker patterns as functions of frequency, and iii) the frequency responses of the linear filters applied

to the loudspeaker signals. We will assign variables to these quantities shortly.

Assume that the array consists of N loudspeakers. The physical system is linear and a frequency domain representation is shown in Figure 1.

We can calculate the output of the system as a linear combination of N **array–basic** patterns. An array–basic pattern we define as the output function response of a single array element (evaluated at a frequency ω). We have a frequency domain linear system relation,

$$y(\theta, \phi; \omega) = z(\omega) \sum_{n=1}^{N} x_n(\omega) h_n(\theta, \phi; \omega),$$

where each $h_n(\theta, \phi; \omega)$ is an array–basic function, $y(\theta, \phi; \omega)$ is the resultant output function, $z(\omega)$ is the Fourier transform of the monophonic input signal evaluated at ω, and $x_n(\omega)$ is the frequency response of the nth filter evaluated at ω.

The patterns are complex functions defined on S^2, the unit sphere. Suppose f and g are two patterns. It isn't difficult to show that the function

$$\langle f, g \rangle = \int_{S^2} f(s) g^*(s) \mathrm{d}s$$

defines an inner–product on the vector space of complex functions on S^2. This integral in spherical coordinates is

$$\langle f, g \rangle = \int_0^{2\pi} \int_0^{\pi} f(\theta, \phi) g^*(\theta, \phi) \sin(\theta) \mathrm{d}\theta \mathrm{d}\phi$$

The integral squared error between pattern f and g then corresponds to

$$\begin{aligned} \text{Error} &= \int_{S^2} |f(s) - g(s)|^2 \, \mathrm{d}s \\ &= \langle f - g, f^* - g^* \rangle \\ &= \|f - g\|^2 \end{aligned} \tag{1}$$

Given an arbitrary pattern g (at a fixed frequency), the gains that minimize the error as defined in Equation (1) between g and an array–realizable pattern f can be calculated as the solution to a linear least squares problem. The system is infinite in the sense that the output is a function, but the least–squares problem is finite and only depends on a Gram matrix involving the desired output, and the array–basic functions. For a good derivation and explanation of least–squares problems involving function spaces, see either [5] or [6]. Evaluation of the entries of the Gram matrix requires integration however, and if the array–basic patterns are derived from measured data, the integrals must be approximated. In this report, we will approximate the integrals by sums of squared error evaluated at points uniformly randomly sampled on S^2.

For notational simplicity, we will suppress dependence on ω, remembering that ω indexes a family of least–squares problems. By sampling the frequency axis we can compute optimal responses $\{x_1(\omega_i), ..., x_N(\omega_i)\}$ at each fixed frequency ω_i. This analysis seeks to determine the patterns that are approximatable under the best possible conditions, i.e., when we are able to specify an arbitrarily complex linear filter for each loudspeaker signal, rendering the sets of responses at different frequencies independently adjustable.

2.2. Continuous and Sampled Least–Squares

Given a desired pattern d, we have that the optimal approximation in the span of $\{h_1, ..., h_N\}$ can be written as

$$d^* = \sum_{n=1}^{N} x_n h_n,$$

where the following equations are satisfied:

$$\sum_{n=1}^{N} x_n \langle h_i, h_n \rangle = \langle h_i, d \rangle, \qquad i = 1, ..., N. \tag{2}$$

Equations (2) are the normal equations. In matrix form, they are

$$Hx = b \tag{3}$$

where $H \in \mathbb{C}^{N \times N}$ and $b \in \mathbb{C}^N$ are defined as

$$\begin{aligned} H_{ji} &= \langle h_i, h_j \rangle \qquad j, i = 1, ..., N \\ b_i &= \langle h_i, d \rangle \qquad i = 1, ..., N \end{aligned}$$

A spatially sampled version of the above problem is derived by first uniformly randomly sampling M

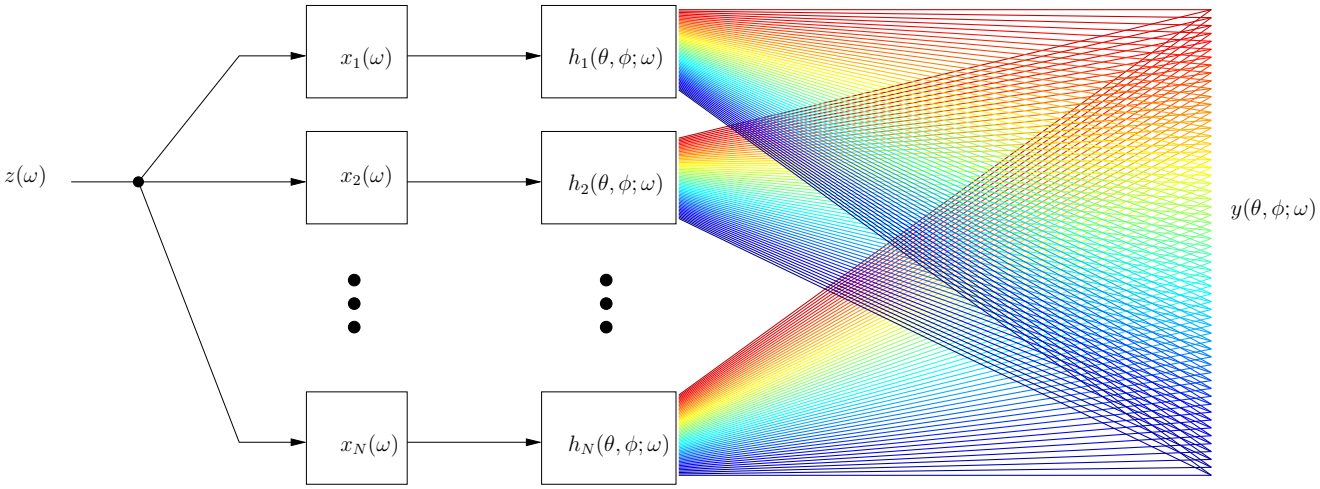

Fig. 1: **Linear System Model.** The input is the Fourier transform of the input signal evaluated at ω (a complex scalar), and the output is a pattern (a complex-valued function of spherical angles (θ, ϕ)).

points from S^2 and creating the vectors

$$\begin{gathered}[h_1(\theta_1,\phi_1),...,h_1(\theta_M,\phi_M)]^T \\ \vdots \\ [h_N(\theta_1,\phi_1),...,h_N(\theta_M,\phi_M)]^T, \quad \text{and} \\ [d(\theta_1,\phi_1),...,d(\theta_M,\phi_M)]^T.\end{gathered}$$

As M increases, the sampled functions approximate more and more closely the continuous functions

$$\begin{gathered}h_1(\theta,\phi) \\ \vdots \\ h_N(\theta,\phi) \quad \text{and} \\ d(\theta,\phi).\end{gathered}$$

The usual vector inner product $h_i^T h_j$ then becomes an approximation to $\frac{M}{4\pi}\langle h_i, h_j\rangle$.

Define the matrix $A \in \mathbb{C}^{M\times N}$, and $d_s \in \mathbb{C}^M$ as follows

$$A = \begin{bmatrix} h_1(\theta_1,\phi_1) & \cdots & h_N(\theta_1,\phi_1) \\ \vdots & \vdots & \vdots \\ h_1(\theta_M,\phi_M) & \cdots & h_N(\theta_M,\phi_M) \end{bmatrix},$$

$$d_s = \begin{bmatrix} d(\theta_1,\phi_1) \\ \vdots \\ d(\theta_M,\phi_M) \end{bmatrix}$$

Then the sampled version of Equation (3) is seen to be

$$A^T A x = A^T d_s. \tag{4}$$

Equation (4) can be constructed and solved easily, the dominating factor in the computation time being the lookup and/or calculation of the sampled functions A and d_s.

To conclude this section on least–squares problems, we want to emphasize that the solution to the normal equations is a linear function of the desired pattern d. This implies that once we know the optimal solution vectors $x_1, ..., x_r$ for several desired responses $d_1, ..., d_r$, we immediately know the solution for any linear combination $\sum \lambda_i d_i$. It is $\sum \lambda_i x_i$.

This linearity is important because it allows us to draw conclusions about the entire uncountable set of radiation patterns by solving problems involving only the countable set of spherical harmonics. It also sometimes allows us to bound errors across sets of patterns defined by continuous control signals, like rotation, by solving finite sets of optimization problems.

We will now look with more detail at the spherical harmonics.

2.3. Spherical Harmonics

The spherical harmonics provide a convenient and natural countable parameterization of the the set of acoustic radiation patterns. By computing the best array–achievable approximations to each spherical harmonic, we can immediately determine the best approximation to a linear combination of spherical harmonics via the same linear combination of solutions, as mentioned in the previous section.

The functions are parameterized by their *degree* l, and *order* m. Figure 2 shows the complex functions plotted up to degree 2. The magnitude is represented as distance from the origin, and phase as a color gradient.

For example the "dipole" corresponds to $l = 1$, $m = 0$. Other orientations of this dipole function can be formed via a weighted combination of patterns drawn from the $l = 1$ grouping. In fact, synthesis of any function composed of $l = 1$ patterns, oriented in any direction, is possible using only the $l = 1$ patterns. This is because the function spaces spanned by harmonics with the same degree are linear subspaces that are invariant with respect to rigid rotation through spatial angles θ and ϕ. See [7], and refer to [8] for an application of this principle in computer graphics. For example, given a pattern that is in the subspace generated by the five degree 2 basis functions, any rotation of that pattern also possesses a spherical harmonic expansion consisting only of degree 2 patterns. Since we wish to control patterns in arbitrary rotational orientations, this decomposition into rotationally invariant subspaces is useful.

Another important property of the spherical harmonics is their orthonormality. Specifically, with respect to the inner product defined above, if f is a spherical harmonic,

$$\sqrt{\langle f, f\rangle} = 1, \tag{5}$$

and if f and g are distinct spherical harmonics,

$$\langle f, g\rangle = 0. \tag{6}$$

Given a particular target pattern, the error as a function of frequency can be determined numerically by discretizing the frequency axis, and solving a set of problems of the form described previously. We would also like to determine how the error generally varies as a function of spherical harmonic degree. In the next section we will discuss the computation of uniform upper and lower bounds on the normalized error, given a *subspace* of desired patterns. Particularly important, because of the reasons above, are the subspaces spanned by spherical harmonics of constant degree.

2.4. Uniform Error

For each harmonic degree, we will compute normalized errors for each of the generating basis functions (i.e., for all the harmonic orders associated with the degree), and will also compute upper and lower bounds on the error given *any* unity norm target pattern in the generated subspace.

Let A be the data matrix, let B be an $M \times D$ matrix, the columns of which are target responses spanning a subspace across which we would like to steer the resulting array patterns. Let $X^\star$ be an $N \times D$ matrix, the columns of which are the optimal loudspeaker signal gains associated with the D target signals. Let λ be a vector consisting of D complex control weights. Because of the linearity of the normal equations, we have that for any λ,

$$\min_x \|Ax - B\lambda\| = \|AX^\star\lambda - B\lambda\| \tag{7}$$

If the columns of B are spherical harmonics, they are orthonormal, and the linear combination $B\lambda$ has norm

$$\|B\lambda\| = \|\lambda\|. \tag{8}$$

Given a subspace spanned by spherical harmonics, the largest approximation error associated with unity gain patterns in the subspace is given by

$$\begin{aligned} &\max_{\|\lambda\|=1} \|AX^\star\lambda - B\lambda\| \\ =&\max_{\|\lambda\|=1} \|(AX^\star - B)\lambda\| \\ =&\sigma_{\max}(AX^\star - B), \end{aligned} \tag{9}$$

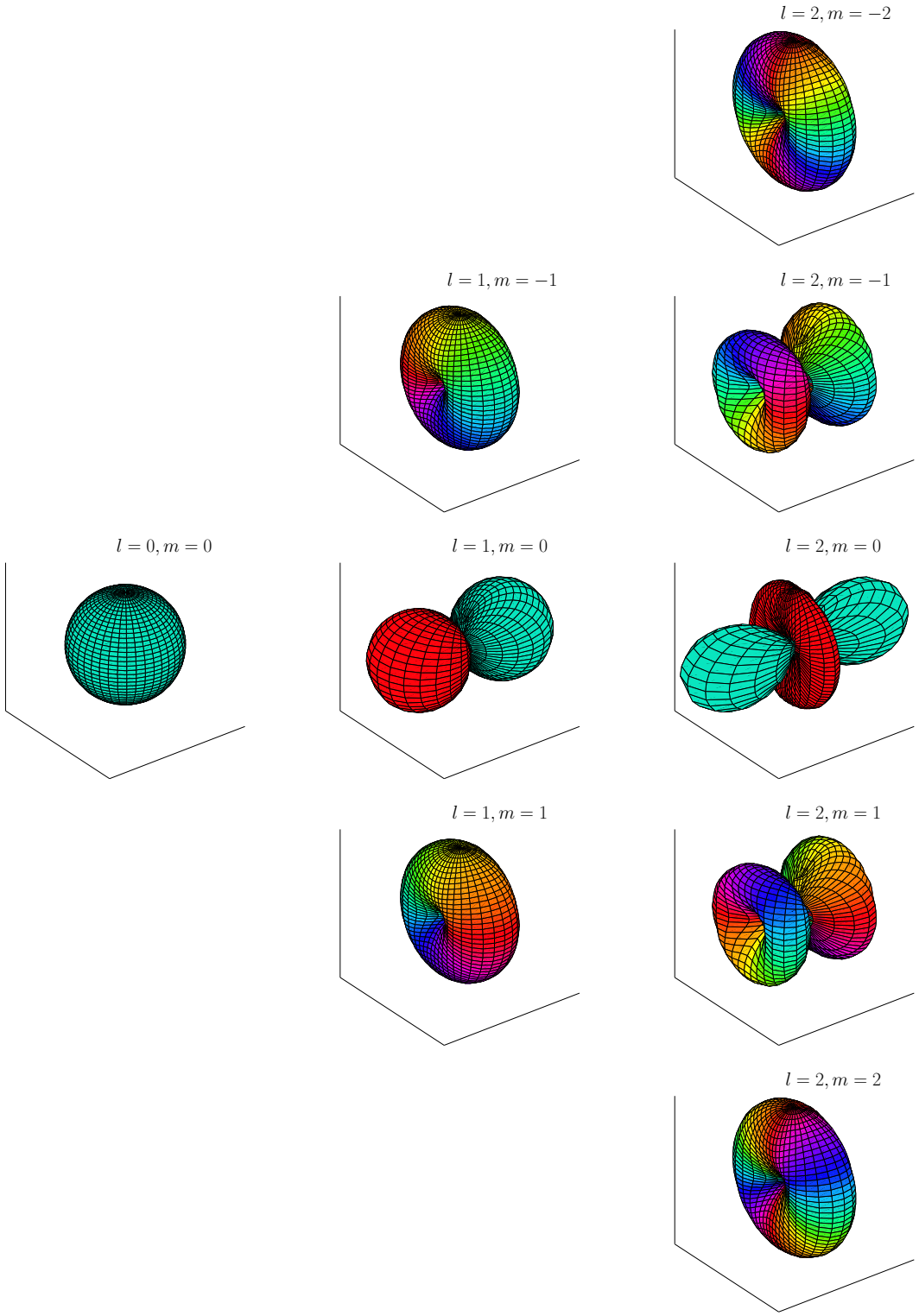

Fig. 2: **Spherical harmonics to degree 2**

where $\sigma_{\max}(AX^\star - B)$ is the maximum singular value of the matrix $AX^\star - B$. Similarly, the smallest approximation error associated with unity gain patterns in the subspace is given by

$$\begin{aligned}&\min_{\|\lambda\|=1} \|AX^\star\lambda - B\lambda\| \\ =&\min_{\|\lambda\|=1} \|(AX^\star - B)\lambda\| \\ =&\sigma_{\min}(AX^\star - B), \end{aligned} \tag{10}$$

where $\sigma_{\min}(AX^\star - B)$ is the minimum singular value.

Geometrically, the set of array–basic functions generate a linear subspace of array–achievable responses. Given a particular desired pattern, the best approximation is its projection onto the array–achievable subspace. Equations (9) and (10) are related to the subspaces generated by the columns of A and B through angles. Intuitively, as the principle angles between the subspaces increases, the normalized error increases accordingly.

Let $Q_A = [Q_{A1}, Q_{A2}]$ and R_A be the QR decomposition of matrix A. Then Q is orthonormal with the columns of Q_{A1} spanning the range of A and the columns of Q_{A2} spanning the nullspace $A^\perp$ of A. See [9], page 228 for properties of the QR decomposition and also see [10]. As treated on pages 239–240 of [9], the error associated with the general full rank least–squares problem $\min \|Ax - b\|$ in terms of the QR decomposition of A is

$$\text{error} = \|Q_{A2}b\|. \tag{11}$$

Applying this to problems (9) and (10), yields

$$\begin{aligned}&\max_{\|\lambda\|=1} \|AX^\star\lambda - B\lambda\| \\ =&\max_{\|\lambda\|=1} \|Q_{A2}B\lambda\| \\ =&\sigma_{\max}(Q_{A2}B) \\ \stackrel{\text{def}}{=}&\cos(\theta_{\max}), \end{aligned} \tag{12}$$

where the last equality follows essentially by the definition of the principle angles between the subspaces spanned by Q_{A2} and (orthonormal) matrix B, i.e., the nullspace of A and the range of B.

Similarly,

$$\begin{aligned}&\min_{\|\lambda\|=1} \|AX^\star\lambda - B\lambda\| \\ =&\cos(\theta_{\min}), \end{aligned} \tag{13}$$

Given a subspace, in particular, a constant degree subspace, upper and lower bounds on the associated least–squares error can be calculated by solving the singular value decomposition problems described above. This is useful because, often control operations can be identified with particular subspaces of patterns. The most clear example of this is rigid rotation which, due to the properties of the spherical harmonics, is associated with constant degree subspaces. Other examples are control strategies involving electronically fading among different sets of patterns. For more applications in optimization involving angles between linear subspaces see also pages 405-410 of [11].

3. RESULTS

The mathematical preparation is complete. In this section we will compute approximation errors associated with spherical arrays. The characterization of the arrays in terms of these errors is dependent on the geometry and the array–basic patterns. The characterizations could be used to assist in the design of an array, or provide guidance when using an existing array. The analysis tells us which patterns are well–synthesizable, and which aren't.

Except in the case involving the constructed dodecahedral array, for which we possess real measurement data, the data in the A matrices is generated by simulating a realistic measurement scenario. Constructing synthetic A matrices allows for comparison among differing array–basic patterns.

3.1. Uniform Bounds Example

Here we provide an example to illustrate the distinction between the uniform error as discussed previously, and error associated with specific target patterns. The example is for a dodecahedral array of diameter approximately 37 cm, with idealized array–basic patterns. The least–squares problem is solved across frequency for each of the seven degree 3 spherical harmonic target patterns, and the error is plotted along with the upper and lower bounds, calculated as described. This example shows that the gap between the bounds can be large. By only looking at the error associated with the spherical harmonic targets, it's not obvious that the there is a wide error spread across the subspace. The upper bound is nearly 1, indicating that there exists a particular pattern, that is a unity–norm combination of the

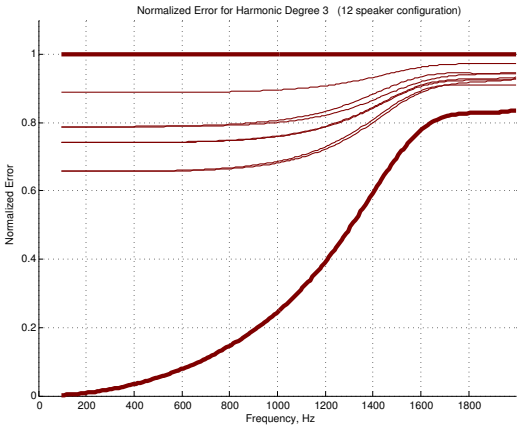

Fig. 3: **Error associated with the degree 3 subspace.** Upper and lower bounds are plotted (bold) along with errors for the seven degree 3 spherical harmonics.

seven basis functions, that is extremely difficult for the array to synthesize. Similarly, there is a pattern that is well-synthesizable, at least at low frequencies. The error associated with spherical harmonic basis patterns lies in between. We can determine the extreme patterns by looking at the singular vectors in the singular value decomposition used to calculate the uniform errors. Intuitively, the existence of extreme patterns is caused by the fact that the array has a particular fixed geometry and orientation. Certain pattern orientations are more or less "aligned" with the geometry of the array. Of course, the situation is subtle, and involves not only the geometry of the array, but the array–basic patterns as well.

3.2. Uniform Error Characterizations

To compare arrays of differing geometries, plots of the error bounds as functions of both frequency and spherical harmonic degree is natural. As the spherical harmonic degree increases, the complexity of the patterns increases. We will compare the uniform error bounds for four spherical arrays. The four arrays are i) a cubic array (6 elements), ii) a dodecahedral array (12 elements), iii) an icosahedral array (20 elements), and iv) a sixty element array (like the icosahedral array, but with 3 elements per triangular face). There are two sets of plots. In the first, we examine the characterizations of the four arrays when the minimum driver spacing is held fixed, and in the second, when the diameter of the arrays is held fixed. In both sets, the array–basic patterns are held fixed. The four configurations are summarized in Tables 1 and 2.

The magnitude of the array–basic patterns used in the simulation is constant across frequency. This is not realistic, but serves to isolate the effects of the geometry on the characterizations of the arrays. A directivity pattern of the array–basic pattern is shown in Figure 4.

Configuration	Number of Drivers	Driver Spacing	Diameter
Cubic	6	19 cm	27 cm
Dodecahedral	12	19 cm	37 cm
Icosahedral	20	19 cm	53 cm
Sixty-Sided	60	19 cm	106 cm

Table 1: Array configurations for plot series 1.

Configuration	Number of Drivers	Driver Spacing	Diameter
Cubic	6	18 cm	26 cm
Dodecahedral	12	14 cm	26 cm
Icosahedral	20	9.3 cm	26 cm
Sixty-Sided	60	4.6 cm	26 cm

Table 2: Array configurations for plot series 2.

3.3. Discussion

Investigating the first series of plots reveals that as the number of drivers in the array increases, more complex patterns can be reproduced. We see additionally that the gap between the upper and lower bounds tends to decrease, and a "cutoff" frequency becomes more easily definable. This makes intuitive sense because an array with a large number of drivers has more degrees of freedom for control. Holding the driver spacings constant (the hypothesis for plot series 1), means the diameter of the arrays with more drivers becomes quite large. Above frequencies with wavelengths corresponding to roughly twice the driver spacing, we see an increase in error.

The second series of plots is for arrays with fixed diameter. In this case, as the number of drivers in

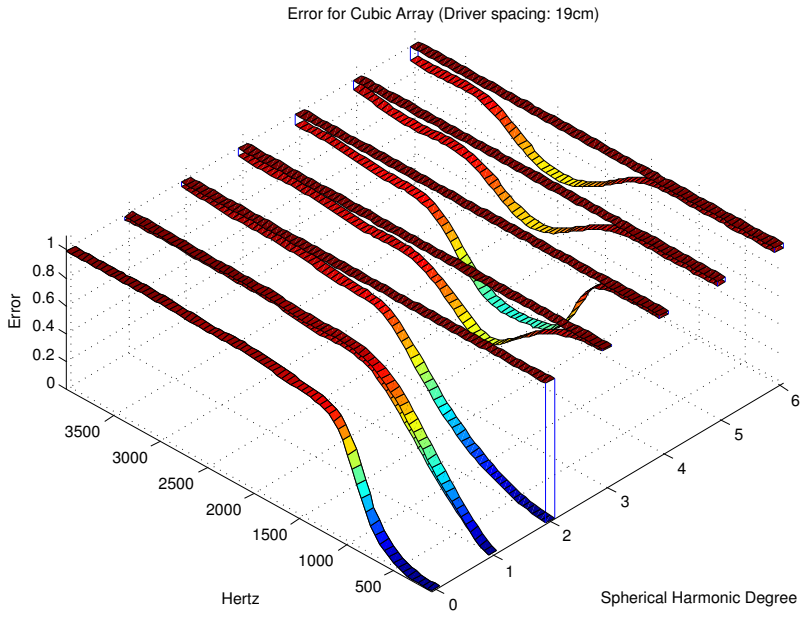

Fig. 5: **Error bounds for cubic array with driver spacing 19 cm.** (Plot series 1)

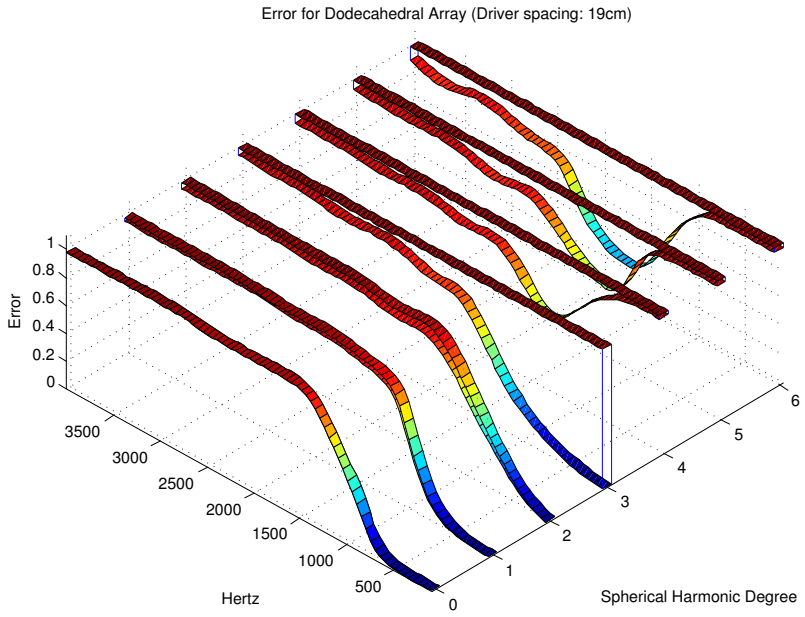

Fig. 6: **Error bounds for dodecahedral array with driver spacing 19 cm.** (Plot series 1)

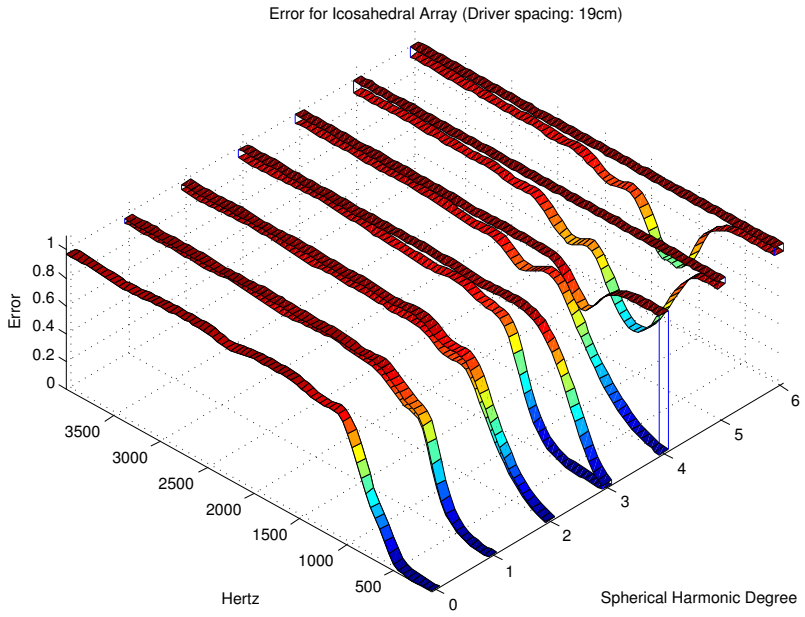

Fig. 7: **Error bounds for icosahedral array with driver spacing 19 cm.** (Plot series 1)

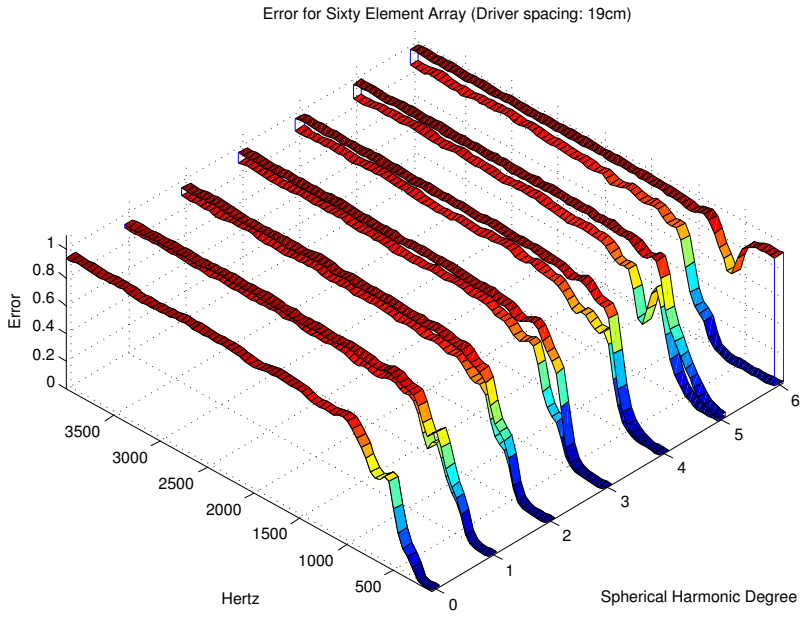

Fig. 8: **Error bounds for sixty element array with driver spacing 19 cm.** (Plot series 1)

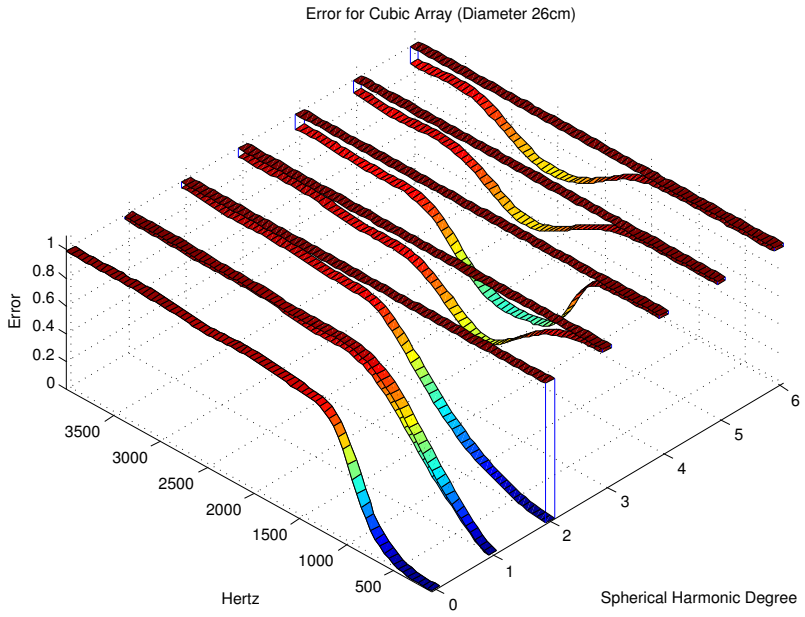

Fig. 9: **Error bounds for cubic array with diameter 29 cm.** (Plot series 2)

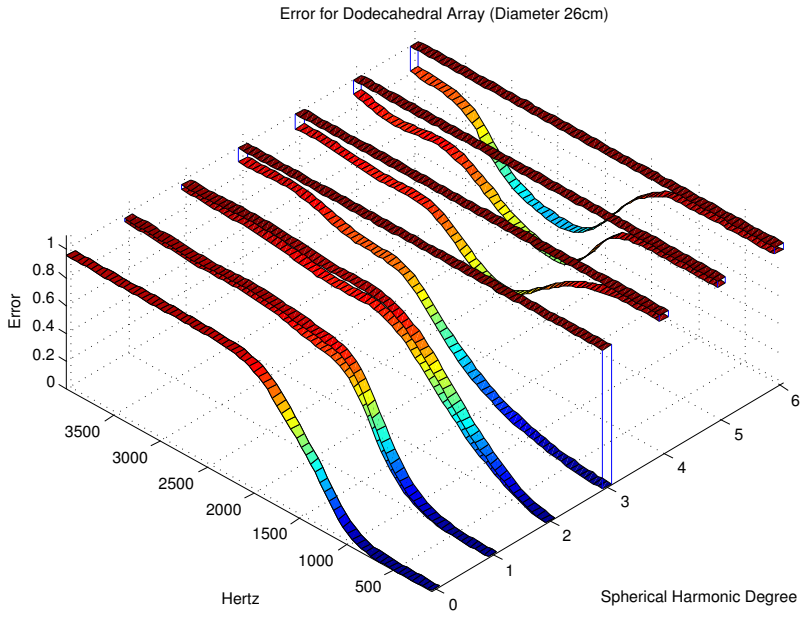

Fig. 10: **Error bounds for dodecahedral array with diameter 26 cm.** (Plot series 2)

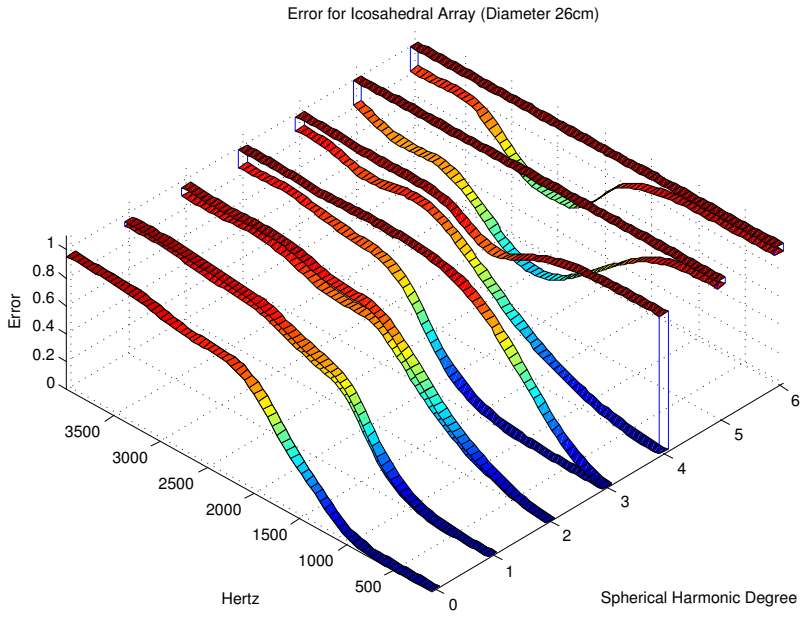

Fig. 11: **Error bounds for icosahedral array with diameter 26 cm.** (Plot series 2)

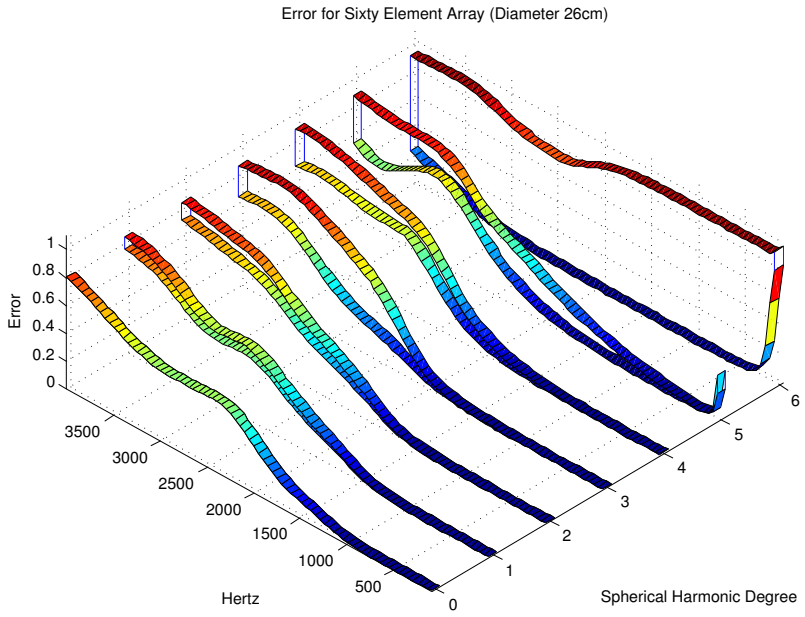

Fig. 12: **Error bounds for sixty element array with diameter 26 cm.** (Plot series 2)

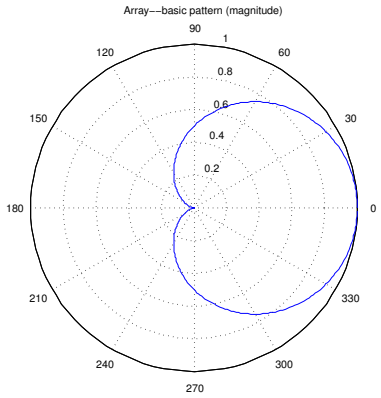

Fig. 4: **Array–basic directivity pattern used in simulation.**(Plot Series 1 & 2)

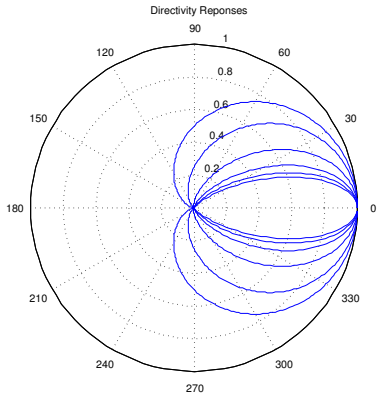

Fig. 13: **Directivity patterns of increasing peakiness** (Used to generate Figure 14)

the array increases, the driver spacings decrease accordingly. The performance of the arrays with more drivers is better both with respect to complexity of patterns and frequency range.

3.4. Array–Basic Patterns

The characterization of the arrays is dependent not only on the geometry of the array, but the array–basic patterns. In this section, we will investigate error bounds for a dodecahedral array with fixed geometry, but for varying array–basic patterns. The variation will be in the peakiness of the directivity response.

Figure 13 shows the magnitude response of the array–basic patterns used to generate the upper bounds in Figure 14. The bounds are for the degree 2 subspace of patterns, and for a dodecahedral array of diameter 37 cm. As the peakiness of the array–patterns increases, the error bound increases at low frequencies, and decreases only slightly at higher frequencies.

Real loudspeaker arrays, of course admit patterns that vary in their directivity across frequency, sometimes very significantly. This has a corresponding effect in terms of the error characterizations.

3.5. Real Dodecahedral Array

In this final section, we will display a characterization of a constructed loudspeaker array, whose array–basic patterns were measured in an anechoic chamber. The error characterizations are predictions of the expected behavior, i.e., they were calculated using the methods described above. The array has diameter approximately 37 cm. We see in Figure 15 that the error varies quasi–periodically with frequency. This is believed to be due to corresponding variation in the array–basic responses across frequency, and is not due to noise.

4. CONCLUSION

We have described in detail an approach to characterizing spherical arrays in terms of error bounds across frequency and spatial complexity indices. These bounds can be seen to be equivalent to best and worst case errors encountered as one electronically steers patterns. Particularly important sets of patterns are the spherical harmonics of increasing degree. Viewed geometrically, these sets of patterns generate linear subspaces that are invariant with respect to rigid rotation.

By solving a series of least–squares problems, we can generate charts of error bounds that, when viewed in aggregate, serve to characterize the expected performance of the array when best synthesizing and controlling prescribed patterns. The interactions of various elements of the system are complex, and in this study, we aim to disentangle some of the effects. At the very least, we hope to provide the reader with a clear method for the evaluation of arrays.

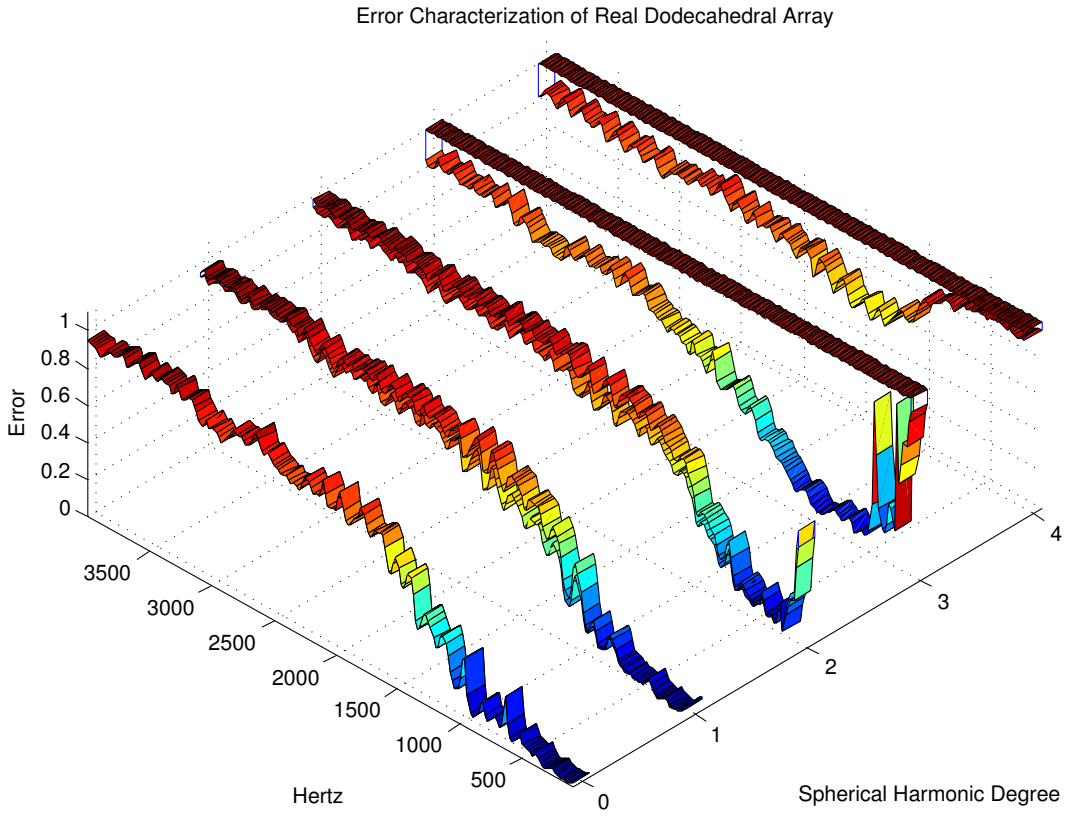

Fig. 15: **Error Characterization for Real Dodecahedral Loudspeaker Array**

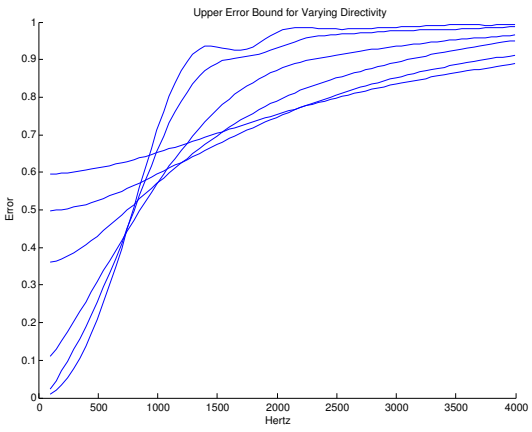

Fig. 14: **Upper Error Bound for Degree 2 subspace, for array–basic patterns of increasing peakiness**

5. ACKNOWLEDGMENT

The authors wish to thank Meyer Sound Laboratories for use of their anechoic chamber, their collaboration with respect to finding solutions to the technical problems described in this paper, and their continued financial support of the work. Support for this project was also provided by a UC Discovery Grant in Digital Media from the University of California's Industry-University Cooperative Research Program (IUCRP). We also want to specifically thank John Meyer, Perrin Meyer, Roger Schwenke, Jon Arneson, Laurent El-Ghaoui, Ervin Hafter, Adrian Freed, Matt Wright, Rimas Avizienis, Richard Andrews, Brian Vogel, Edgar Berdahl, and Lieven Vandenberghe.

6. REFERENCES

[1] Olivier Warusfel, Philippe Derogis, and Rene Caussé. Radiation synthesis with digitally controlled loudspeakers. *Presented at the 103rd AES Convention*, 1997.

[2] A.J. Berkhout, D. de Vries, and P. Vogel. Acoustic control by wave field synthesis. *Journal of the Acoustical Society of America*, 93(5):2764–2779, May 1993.

[3] David T. Blackstock. *Fundamentals of Physical Acoustics*. John Wiley & Sons, Inc., 2000.

[4] Leo L. Beranek. *Acoustics*.

[5] E. W. Cheney. *Approximation Theory*. Chelsea, 2nd edition, 1982.

[6] David G. Luenberger. *Optimization by Vector Space Methods*. John Wiley and Sons, Inc., 1969.

[7] Zhengwei Su and Philip Coppens. Rotation of real spherical harmonics. *Acta Crystallographica Section A*, A50:636–643, 1994.

[8] Michael Kazhdan, Thomas Funkhouser, and Szymon Rusinkiewicz. Rotation invariant spherical harmonic representation of 3d shape descriptors. In *Proceedings of the Eurographics/ACM SIGGRAPH symposium on Geometry processing*, pages 156–164. Eurographics Association, 2003.

[9] Gene H. Golub and Charles F. Van Loan. *Matrix Computations*. Johns Hopkins University Press, 3rd edition, 1996.

[10] Lloyd N. Trefethen and David Bau III. *Numerical Linear Algebra*. Society for Industrial and Applied Mathematics (SIAM), 1997.

[11] Stephen Boyd and Lieven Vandenberghe. *Convex Optimization*. Cambridge University Press, 2004.